ACS NANO

www.acsnano.org

ARTICLE

Self-Organizing Arrays of Size Scalable Nanoparticle Rings

Ying Bao,[†,‡] Thomas A. Witten,[†,§] and Norbert F. Scherer*[,†,‡]

[†]Department of Chemistry, [‡]The James Franck Institute, [§]Department of Physics, The University of Chicago, 929 East 57th Street, Chicago, Illinois 60637, United States

Supporting Information

ABSTRACT: A central challenge in nano- and mesoscale materials research is facile formation of specific structures for catalysis, sensing, and photonics. Self-assembled equilibrium structures, such as three-dimensional crystals or ordered monolayers, form as a result of the interactions of the constituents. Other structures can be achieved by imposing forces (fields) and/or boundary conditions, which Whitesides termed "self-organization". Here, we demonstrate contact line pinning on locally curved surfaces (*i.e.*, a self-assembled monolayer of SiO_2 colloidal particles) as a boundary condition to create extended arrays of uniform rings of Au nanoparticles (NPs) on the SiO_2 colloids. The mechanism differs from the well-known "coffee-ring" effect; here the functionalized NPs deposit at the contact line and are not driven by evaporative transport. Thus, NP ring formation depends on the hydrophobicity and wetting of the SiO_2 colloids by the chloroform solution, ligands on the NPs, and temperature. The NP rings exhibit size scaling behavior, maintaining a constant ratio of NP ring-to-colloid diameter (from 300 nm to 2 μm). The resultant high-quality NP ring structures are expected to have interesting photonic properties.

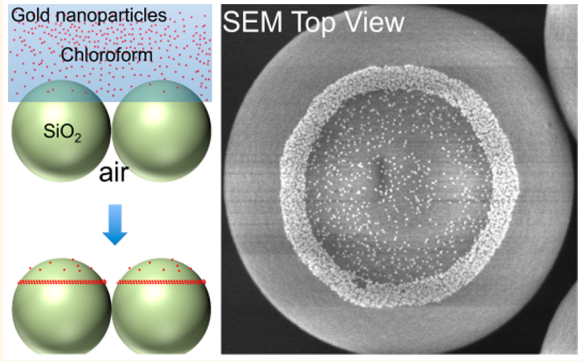

KEYWORDS: *nanoparticle rings, SiO_2 monolayer, wetting, contact line, scaling behavior*

Beyond their aesthetic appeal, ring-like materials have received significant attention over a wide range of real-world cases and technological applications due to their structural symmetry and interesting properties.[1−3] For example, the bacterial light-harvesting assemblies, LH1 and LH2, have ring structures to facilitate excitation transport.[4,5] Ring-like superconductors can sustain "persistent currents",[6] while metallic rings yield optical resonance properties and special magnetic responses, which make them promising for application in sensing and data storage.[7−9] Recently, micrometer to nanometer scale ordered ring-like structures have received increasing interest for device miniaturization.[3,10−12] For example, ultracompact subwavelength waveguides, including interferometers and ring resonators, were fabricated with ring-like structures for large-angle bending and splitting of radiation.[10] Therefore, robust methods to fabricate large arrays are required to further device development and miniaturization.

Ring-like nanostructures have been prepared using various approaches such as e-beam lithography, microcontact printing, and colloidal templating.[13,14] However, lithography, including evaporating metals on an array of colloidal particles,[15] and microcontact printing can be complex and challenging to obtain nanometer precision over large scales. Alternatively, processes involving direct manipulation of nanomaterials might cause mechanical damage to the ring-like structures that would alter their physical properties in addition to the difficulty of creating large numbers of repeated structures.[16] Bottom-up self-assembly and self-organization of nanoparticles (NPs) into ordered structures have the potential for parallel fabrication of particular structures with nanoscale precision at relatively low cost.[7,17−26] Self-assembly of NPs into ring-like nanostructures has been accomplished using several approaches. Using water droplet templates[17] resulted in a high yield of ring structures but lacked control of ring size and location over the entire substrate. Therefore, precisely fabricating well-ordered arrays of NP-based ring-like nanostructures with scalable sizes in an efficient and simple manner is still an open challenge.

In the present paper, we report a surprisingly simple method that achieves these goals. Our approach involves NPs in solution attaching to the boundaries defined by the contact line of a solvent that is pinned on locally curved surfaces. The local curvature is provided by nano-to-microscale SiO_2 colloid spheres that are readily self-assembled into ordered monolayers. These colloids guide the formation of an ordered array of NP

Received: July 25, 2016
Accepted: August 30, 2016
Published: August 30, 2016

DOI: 10.1021/acsnano.6b04965
ACS Nano 2016, 10, 8947−8955

rings. The driving force for NP transport and self-organization depends mainly on NP segregation at the liquid−air interface and to a lesser degree on the motion of the drying front. Therefore, the morphology (*i.e.*, rings *vs* disordered particle coatings) can be controlled by the experimental parameters such as substrate temperature, NP concentration, packing of the SiO_2 colloid monolayers, and the ligands on the NPs. The sizes of the resulted rings are primarily determined by the size of the SiO_2 colloids and the humidity. The arrays of NP rings can be formed over regions several tens of mm^2 in size. Here, we demonstrate NP ring formation with suitably functionalized Au NPs (~10 nm dia.). However, the process also works for a range of suitably functionalized metal and semiconductor NPs.

RESULTS AND DISCUSSION

In a typical Au NP self-organization experiment, as shown in Figure 1, a small volume of the Au NP solution is deposited on the SiO_2 colloid monolayer (which is itself formed on a Si substrate), and the chloroform solvent is allowed to evaporate at a selected temperature (details in the Methods Section).

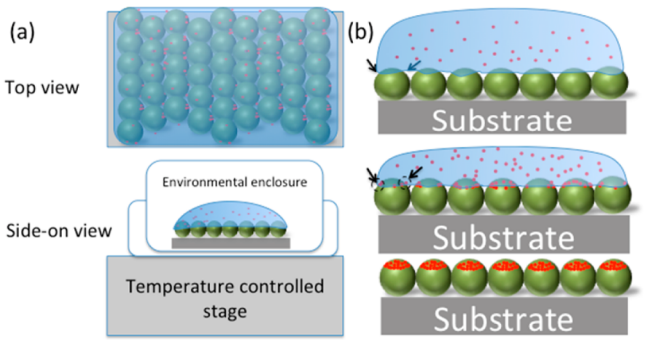

Figure 1. Schematic of the self-organization experiment (not to scale). (a) The experimental set up for depositing NPs on a self-assembled monolayer of SiO_2 spheres. (b) An overview of Au NP deposition on a monolayer of SiO_2 spheres as ring-like structures. A drop of Au NP/chloroform solution (blue) covers the surface of the monolayer of SiO_2 spheres (green) and is allowed to evaporate. The evaporation of solvent causes NPs to both deposit and to increase in concentration in the remaining chloroform solution. Under the correct conditions, NPs deposit at the pinned chloroform-SiO_2 contact line. Eventually, the solvent will have completely evaporated leaving the Au NPs deposited on each SiO_2 sphere. Large regions of the SiO_2 colloid array are coated with highly uniform Au NP ring structures.

Temperature Dependence. The morphologies of the resultant samples were examined by SEM. Figures 2a and S1 reveal that Au@MT$(PEG)_4$ NPs (diameter ~10 nm, deposition at 21 °C and 50% relative humidity (RH)) are randomly deposited over the entire surface of the SiO_2 colloids (diameter ~600 nm). Such a NP coating reflects significant wetting of the dispersing medium; the contact angle of chloroform to SiO_2 is <10° at room temperature, which means that it can fully wet the SiO_2 spheres.[27] Even the Si wafer substrate supporting the monolayer of SiO_2 spheres was coated with Au NPs (Figure S1). Figure 2b shows the results of another experiment (also performed under ~50% RH), but with the substrate heated to 60 °C while the colloidal solution evaporates. Here, as well as in Figure S2, the Au NPs form string-like structures on the SiO_2 surface. The string-like features are reminiscent of kinetic-driven aggregation, which is more likely at 60 °C than at 21 °C because the solvent evaporation is much faster; <1 min at 60 °C *vs* ~10 min at 21 °C.[28] Similar types of lateral aggregation of NP formation were also observed in previous reports.[29,30]

By contrast, Au NP deposition is remarkably different when conducted using a cooled substrate adjusted to near 0 °C with an ice bath. As shown in Figure 2c, the Au NPs self-organize into ring-like structures that are deposited only on the top hemisphere of individual SiO_2 spheres; no NPs are deposited outside of the rings or on the Si substrate. Furthermore, the ring structures form over a major fraction of the SiO_2 colloid monolayer substrate. Figure 2d shows a larger region (~3 × 3 μm^2) of the sample. The drastically different structures in Figures 2c,d *vs* 2a,b suggest a large change of the wetting behavior of chloroform (*i.e.*, the chloroform solutions) at the lower temperature. It is known that SiO_2 spheres are poorly wetted by chloroform at 0 °C due to their hydrophobicity. In fact, chloroform does not wet the entire surface of the SiO_2 sphere monolayers; the chloroform containing Au NP solution is located only on the top of the SiO_2 spheres at near 0 °C as depicted in Figure 1b. These results clearly demonstrate that the interfacial energy between the chloroform and the SiO_2 surface varies with temperature. We will demonstrate below that the formation of Au NP rings is related to the strong pinning force at the chloroform-SiO_2 contact line.

The wetting behavior of chloroform at 0 °C and ~50% RH was further studied on sparsely deposited SiO_2 spheres of ~2 μm diameter. Figure 3a−c shows that the Au NPs were deposited either on the Si substrate, but only starting a significant distance away from the isolated SiO_2 spheres, or on the surface of SiO_2 spheres as ring-like structures. On the Si substrate, Au NPs were densely packed at the "edge of a bubble" and sparsely deposited at larger distances. The location and size of the Au NP ring structures on the SiO_2 spheres vary depending on the local packing condition of the SiO_2 spheres and the proximity of each SiO_2 colloid to the perimeter of the cluster (see Figure 3b,c). Specifically, the SiO_2 spheres that are packed with neighboring spheres have Au NP ring structures that are similar to what we observe on monolayer samples (Figure 2c,d). However, the SiO_2 spheres located at the periphery of a group have larger ring structures that might also be skewed off center of the sphere. These results demonstrate that chloroform poorly wets the SiO_2 spheres at 0 °C and in fact only contacts the top hemisphere of the spheres. From Figure 3b,c, it is readily apparent that the chloroform solution smoothly extends as a dome of small curvature to the Si substrate enclosing a vapor bubble. Therefore, a contact line was formed on each SiO_2 sphere. It is important to note that an ordered monolayer of SiO_2 spheres is not necessary for the formation of Au NP ring structures.

Scaling of Au NP Ring Size. The effect of SiO_2 sphere size on the Au NP ring structure was investigated using SiO_2 spheres from 300 nm to 2 μm diameter (all values are summarized in Table 1). Three sizes of SiO_2 spheres with mean diameters of 306 ± 23, 556 ± 22, and 693 ± 21 nm at ~50% RH and three sizes of SiO_2 spheres with mean diameters of 378 ± 24, 554 ± 20, and 1775 ± 54 nm at ~35% RH were used to fabricate high-quality SiO_2 monolayers for the preparation of Au NP coatings and ring structures. SEM images (Figure 4a−f) show that Au NP ring structures formed on all samples at 0 °C. We define the relative size, r, as the ratio of ring radius (R) to SiO_2 sphere radius (L); *i.e.*, $r_i = R_i/L_i$ for each colloid of type i, as illustrated in Figure 4g. Scatter plots of the scaled ring radius r_i, to scaled SiO_2 colloid radius $L_i/\langle L_i \rangle$, are shown in Figure

DOI: 10.1021/acsnano.6b04965
ACS Nano 2016, 10, 8947−8955

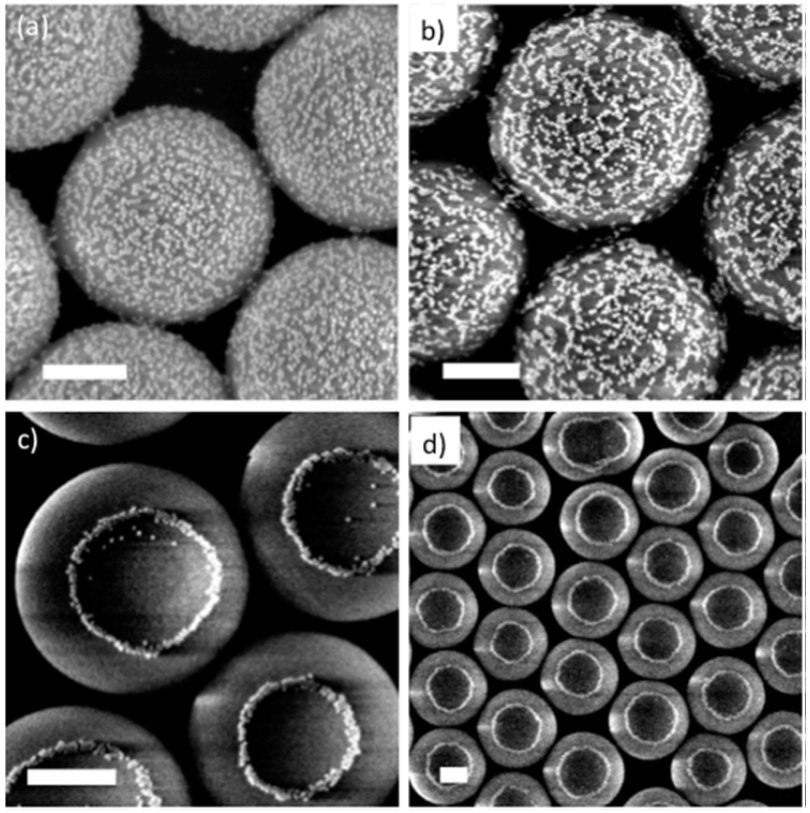

Figure 2. SEM images of various Au@MT(PEG)$_4$ NP structures formed as a function of substrate temperature. (a) SEM image of Au NPs on SiO_2 spheres under ~50% RH and the substrate maintained at 21 °C during evaporation. (b) SEM image of the formation of Au NPs on SiO_2 spheres at ~50% RH and the substrate maintained at 60 °C during evaporation. (c) SEM image of the formation of Au NPs on SiO_2 spheres at ~50% RH and substrate at 0 °C during evaporation. (d) A zoomed-out SEM image of (c). The Au NPs are the bright dots, strings or rings in the images. All scale bars are 200 nm.

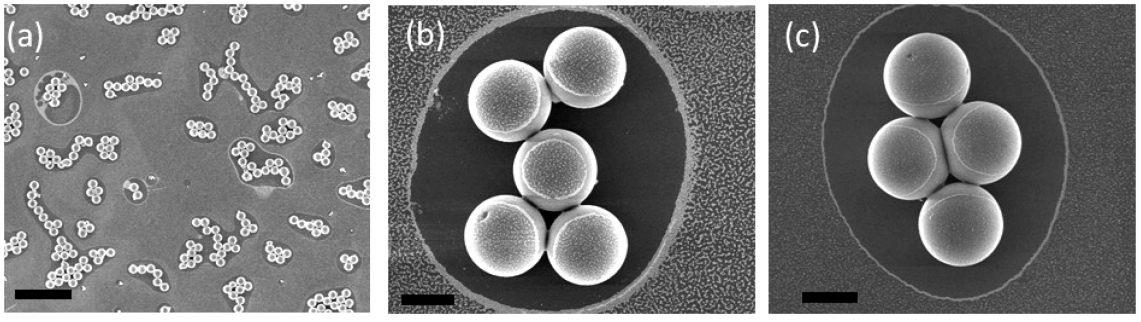

Figure 3. SEM images of formations of Au@MT(PEG)4 NPs on a sparsely deposited SiO_2 sphere (with diameter ~2 μm) sample, which was prepared under 35% RH and the substrate temperature was kept at 0 °C. (a) Low- and (b, c) high-magnification SEM images. Scale bars: (a) 10 and (b, c) 1 μm. (Analogous results are obtained for other size SiO_2 colloids.)

4h,i. The relative sizes of the Au NP rings are r_i = 0.47, 0.57, and 0.51 for the 306, 556, 693 nm SiO_2 sphere samples at ~50% RH and r_i = 0.64, 0.63, and 0.64 for the 378, 554, 1775 nm sphere samples at ~35% RH, respectively. Note, the evaporation rate of chloroform under these relative humidity conditions should be the same by Dalton's law. The close agreement of the measured values of r_i for each humidity condition shows that the formation of Au@MT(PEG)$_4$ NP rings occurs for a wide range SiO_2 sphere sizes. Moreover, Figure 4h,i which shows that the ratio of Au NP ring radius to SiO_2 sphere radius is constant under same relative humidity condition, regardless of SiO_2 sphere radius. This demonstrates size scaling (with the mean as the scaling parameter). That is, the self-organization of Au NP rings is a scale-free phenomenon.

Furthermore, the size of the Au NP ring on a given SiO_2 sphere also depends on the packing of the nearby SiO_2 spheres and thus varies in certain ranges associated with the polydispersity and packing quality of the SiO_2 spheres. For example, for 306 nm diameter SiO_2 spheres, the Au NP rings indicated by red arrows in Figure 4a have significantly smaller radii than the surrounding rings. Therefore, since the 306 nm SiO_2 spheres have a greater polydispersity than the other ones (Figure 4h), there is greater scatter in R/L. Conversely, the monolayers of the larger size SiO_2 spheres are more uniform and better packed, and thus the distributions of Au NP ring diameters are narrower. This conclusion is further confirmed by

DOI: 10.1021/acsnano.6b04965
ACS Nano 2016, 10, 8947–8955

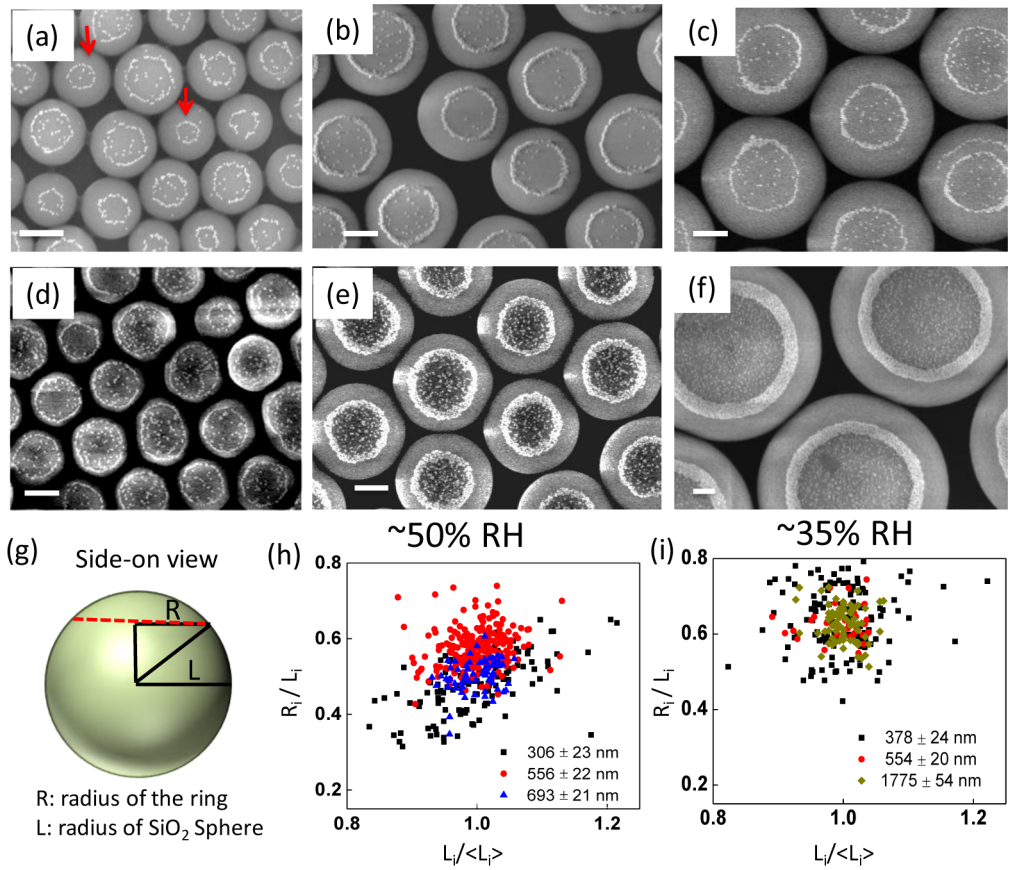

Figure 4. SiO_2 size impacts the properties of the Au NP ring structures. (a–f) SEM images of Au NP rings on the monolayers prepared, separately, with SiO_2 spheres of three sizes. Their mean diameters: (a) 306 ± 23, (b) 556 ± 22, (c) 693 ± 21, (d) 378 ± 24, (e) 554 ± 20, and (f) 1775 ± 54 nm. Scale bar: 200 nm. (g) a schematic side view of a SiO_2 sphere, defining $r = R/L$; (h,i) R_i/L_i plotted against $L_i/\langle L_i\rangle$, for SiO_2 monolayer substrates with $\langle L_i\rangle$ = 306, 556, 693 nm at ~50% RH and $\langle L_i\rangle$ = 378, 554, 1775 nm on the ~35% RH, respectively.

Table 1. Parameters for Au NP Ring Formation

relative humidity	SiO_2 diameter (nm)	ratio (R/L)	relative standard deviation (L, R/L)
~50%	306 ± 23	0.47 ± 0.08	(7.5%, 17.9%)
~50%	556 ± 22	0.57 ± 0.06	(4.0%, 10.0%)
~50%	693 ± 21	0.51 ± 0.05	(3.0%, 10.4%)
~35%	378 ± 24	0.64 ± 0.09	(6.4%, 13.6%)
~35%	554 ± 20	0.63 ± 0.05	(3.7%, 7.3%)
~35%	1775 ± 54	0.64 ± 0.05	(3.0%, 8.3%)

the relative standard deviation (RSD) of relative ring sizes (R/L) *vs* RSD of SiO_2 sphere diameters (L) shown in Figure S3. The yellow shaded region of Figure S3 highlights the larger RSDs of L (7.5%, 6.4%) associated with the smaller SiO_2 spheres (306 nm, 378 nm dia.) that exhibit larger RSDs of R/L (17.9%, 13.6%), while the blue shaded region highlights the more uniform samples (554 nm, 556 nm, 693 nm, 1775 nm dia.) with smaller RSDs of L that exhibit smaller RSDs of R/L; the (L, R/L) are (4.0%, 10.0%); (3.0%, 10.4%), (3.7%, 7.3%); (3.0%, 8.3%), respectively.

These dependences of ring size and ring position on the SiO_2 colloid correspond well to the expected shifts in the chloroform solution contact lines on the SiO_2 spheres. For example, we show in the geometrical model in the Supporting Information that when a large sphere is adjacent to a smaller one, its contact line should be displaced toward its neighbor. Likewise, the contact line on the smaller sphere is displaced away from its larger neighbor. Thus, the contact line for a smaller sphere surrounded by larger ones is displaced away from its neighbors in all directions and thus contracts, as shown in Figure 4a.

Au NP Concentration Dependence. The concentration of the Au NP colloidal solution also plays a role in Au NP ring formation on SiO_2 spheres. Figure 5a–c shows SEM images of Au NP rings obtained for three different Au NP colloid concentrations (number densities) in chloroform. It is clear that Au NP rings are not affected by the Au NP concentration. All ring-like structures formed at various Au NP concentrations exhibit the same relative size, r. The distributions of the relative size, r, at different Au NP concentrations are shown in Figure 5d. From Gaussian fitting, the distributions for the three cases are centered at 0.61 ± 0.05, 0.55 ± 0.04, and 0.57 ± 0.05, respectively, indicating that the relative size of the rings is not affected by the Au NP concentration in solution. On the other hand, the concentration of Au NPs does impact their deposition and density within the boundary of the Au NP ring. There are few or no NPs observed inside the rings (Figure 5a), when a low concentration Au NP solution is used. The number of interior NPs increases with concentration, as does the width of the ring annulus.

The location and motion of the chloroform drop on the SiO_2 spheres can affect the details of the density of Au NPs deposited and presumably also their transport in the droplet. We monitored the progression of the chloroform drop shape and volume during evaporation at 21 °C and ~50% RH. The motion of a chloroform drop (Movie S1) clearly shows that it

DOI: 10.1021/acsnano.6b04965
ACS Nano 2016, 10, 8947–8955

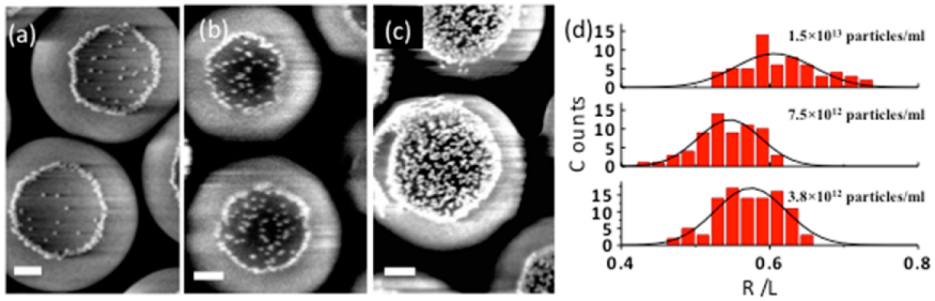

Figure 5. Impact of concentration on the properties of the Au NP ring structures. Samples were 556 ± 22 nm SiO_2 spheres with 10 nm Au NP, prepared under 50% RH and 0 °C substrate temperature. (a–c) SEM images of Au NP rings assembled with various concentrations of Au NPs in solution. Number densities: (a) 3.8 × 10^{12}, (b) 7.5 × 10^{12}, and (c) 1.5 × 10^{13} particles/mL. Scale bar: 100 nm. (d) Relative sizes, $r = R/L$ plotted for different concentrations of Au NP colloids in solution.

shrinks to smaller size, and the contact angle on the SiO_2 colloid monolayer remains unchanged throughout. Thus, the chloroform drop shrinks to maintain the contact angle and does not spread (Movie S1).

Therefore, the density of Au NPs on the surface varies across the entire substrate due to more rapid reduction of the solution volume *vs* the rate of Au NP deposition. That is, the Au NP solution becomes more concentrated as the evaporation of the chloroform solution proceeds. Figure S4 shows SEM images from various locations on the SiO_2 monolayer. It is obvious that the density of Au@MT(PEG)$_4$ NPs is increasing from the edge to the center as the solvent evaporates. We confirmed this by taking SEM images on the edge and near the center of the samples (Figure S4). Depending on the initial Au NP concentration, regions a–d will have different relative areas on the substrate as expected.

Surface Wetting and Hydrophobicity. The way that chloroform wets the SiO_2 spheres is related to the interfacial energy between the chloroform and the SiO_2 surface. In our experiments, condensation of water on the surface of the SiO_2 spheres at near 0 °C would affect the interfacial energy, wetting behavior, and contact angles.[31] To demonstrate the importance of water condensation, a control experiment was conducted under continuous nitrogen purge while the substrate was cooled to 0 °C so that the particle deposition occurs in the absence of humidity. As shown in Figure S5, no Au NP ring structures form on the SiO_2 spheres! This result indicates that a condensed layer of water forms on the surface of SiO_2 spheres as the freezing point of water is approached (*i.e.*, below the dew point) and that this plays a key role in Au NP ring formation. It should be emphasized that the morphology is due to the relative humidity instead of the evaporation rate; while the evaporation rate is faster under the nitrogen purge condition than other relative humidity conditions (~35% RH, ~ 50% RH), the evaporation is also faster at elevated temperatures where NP rings do not form.

To further confirm the role of surface hydrophilicity on the formation of Au NP ring structures, we altered the ligand coating on the Au NPs. Figure 6a,b shows that dodecanethiol-coated Au NPs (Au@DDT NPs) organize into "compact mound" structures under the same experimental conditions (the substrate cooled to 0 °C, ~ 50% RH at 21 °C in the lab). This result is in striking contrast to the rings formed for PEG-coated Au NPs and confirms that the different affinity of Au NPs, with hydrophilic or hydrophobic ligands, to SiO_2 (and the water layer coating SiO_2) determine the type of Au NP structures formed.

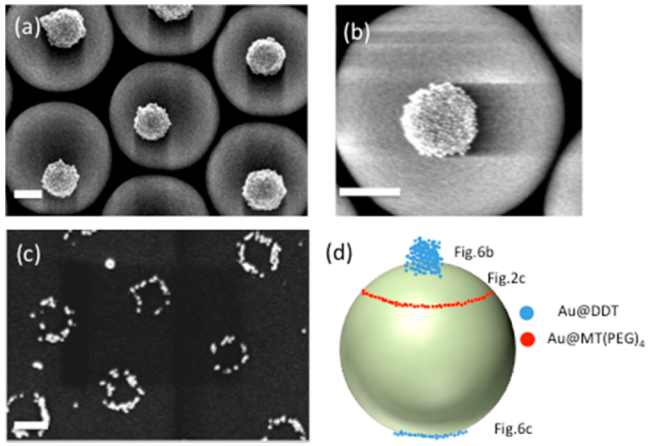

Figure 6. Impact of humidity and ligands on Au NP-SiO_2 interactions. (a, b) Low- and high-magnification SEM images of Au@DDT NPs forming compact Au NP mounds under ~50% RH, substrate at 0 °C. (c) SEM image of Au@DDT NPs forming rings beneath the SiO_2 colloids under ~50% RH, substrate at 21 °C. Scale bar: 200 nm. (d) Schematic of Au NP structures formed: Au NP ring-like structures as in Figure 2c, compact mound structure as in (b) and ring formation as (c) are depicted relative to where they form on or near an SiO_2 colloid.

Given the hydrophobic nature of the Au@DDT NPs, there should only be a weak interaction between them and the water coated SiO_2 surface. Since we did not find any Au@DDT NPs on SiO_2 spheres at the outer edge of the chloroform drop, we deduce that in the early stage of chloroform evaporation, the Au@DDT NPs remain in the solvent rather than attach to the contact line. In the later stage of evaporation, when the Au@DDT NPs become over saturated in the chloroform solvent, nucleation events will occur, and Au@DDT NPs will precipitate from the solvent. The nucleated Au@DDT NPs self-assemble into a close packed structure in order to minimize their overall energy, analogous to the colloidal microscopic "soccer balls" formed when evaporating a hydrophilic colloidal solution on a superhydrophobic surface.[32] Thus, we observe small compact mounds of Au NPs, as shown in Figure 6a,b. Ultimately, at the completion of chloroform evaporation, there are large accmulations of Au@DDT NPs. Figure S6 is an SEM image taken at the center of the sample showing a region that has both the compact mounds on selected SiO_2 spheres and continuous Au@DDT NPs aggregations at the end of evaporation. The compact mounds are not correlated to

DOI: 10.1021/acsnano.6b04965
ACS Nano 2016, 10, 8947–8955

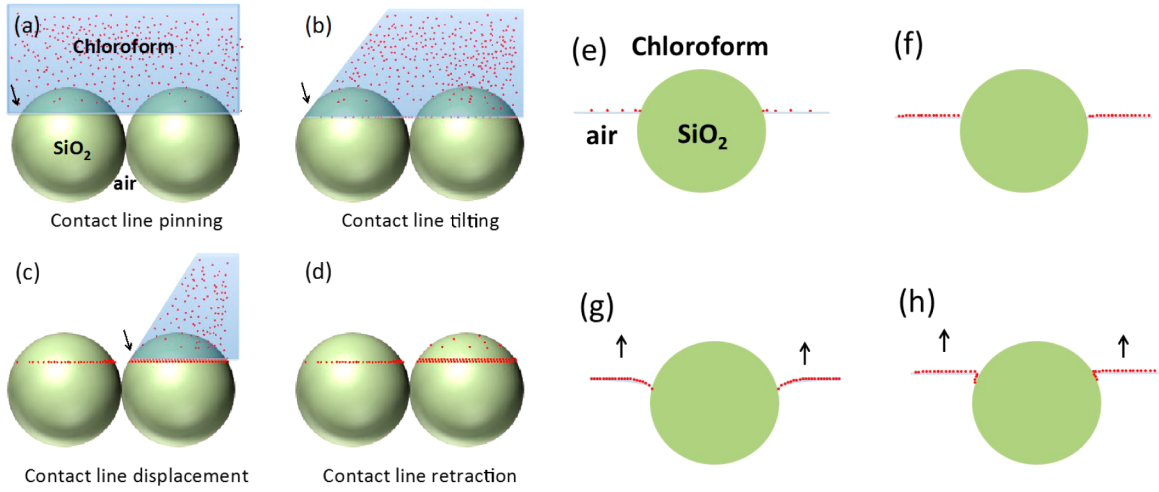

Figure 7. A schematic representation of our proposed mechanism for the evaporation of Au NP (red dots) solution on the boundary of the sample (arrows indicate the change of the contact line) (a–d) and mechanism of contact line pinning (and rising) and for the deposition of Au NP (red dots) to form Au NP rings (e–g) (not to scale): (a) initial fluid shape; (b) evaporation occurs, and the deposited NPs at contact line pin the meniscus and allows the contact angle to decrease; (c) when the contact angle reaches zero, the meniscus shifts to the adjacent sphere; and (d) any NPs bound to the sphere at the contact line would be left behind without solvent as the contact line rises, resulting in a dense ring deposit. Note that multiple concentric rings can form for sufficient NP concentration. (e) Initial fluid shape, Au NP adsorb to the solvent–air interface; (f) over time, adsorption increases and creating a dense NP layer on the interface; (g) adsorbed layer decreases the air–solvent interfacial energy causing the contact line to rise on the spheres; and (h) with the air–solvent interfacial energy decrease, the contact line rises on the SiO_2 spheres, and the particles at the contact line are pushed onto the sphere at progressively higher latitudes.

individual SiO_2 spheres and also reside in the gaps between SiO_2 spheres, as indicated by the arrows in Figure S6.

We also conducted an experiment with Au@DDT NPs at 21 °C and found that the hydrophobic Au NPs rarely deposit on the surface of the SiO_2 spheres. By removing the monolayer of SiO_2 spheres (*i.e.*, lift off using Scotch tape, see Methods) after evaporation of the chloroform solution, we find that the Au NPs prefer to form rings beneath the SiO_2 spheres on the Si substrate (Figure 6c), as has been observed by others.[33] This result is not surprising considering the hydrophobicity of the colloidal solution and the Si substrate. Therefore, it is clear that the ligand on the Au NPs strongly affects the interaction of NPs with the SiO_2 spheres, and these interactions are extremely important in the formation of the Au NP ring structures. Figure 6d schematically summarizes these observations.

Au NP Deposition and Mechanism of Ring Formation. Figure 1 summarizes the mechanism of ring formation. The NP rings form at the contact line where the fluid meniscus meets the spheres. However, it leaves an open question of how the Au NPs in the fluid drop travel to the contact line and then form the rings. One possible mechanism is that the solvent will leave individual micro- or nanodroplets on each SiO_2 sphere during evaporation, and transport occurs within these to the contact line forming the Au NP ring-like structures. However, the creation of individual microdroplets from the initial chloroform drop, which extends over macroscopic scales, requires kinetic detachment events. There is also the issue of the large energy cost associated with forming (sub)micro-scale chloroform droplets with high curvature on each SiO_2 colloid. Therefore, we view this mechanism as unlikely. Another possible mechanism considers the ring formation as analogous to the "coffee-ring effect"[16] seen in macroscopic sessile drops on a solid surface. In the coffee-ring effect, solute particles are transported to the contact line by an outward capillary flow throughout the drop. This results in a strongly concentrated deposit at the contact line. The contact lines in our system resemble these coffee stains. However, in the present case, most of the evaporation occurs at the outer perimeter of the drop and perhaps some from beneath for the spheres near the edge of the droplet. However, for the spheres in the inner region, little to no evaporation can occur from below. Therefore, we favor the view that *mainly nonevaporative effects create the NP rings*. As Figure 3 shows, the rings form even when the spheres are confined in a small air bubble. Here, no (or very slow) evaporation in the bubble is expected, yet the rings form.

The retraction of the drop of chloroform solution involves evaporation, retraction, and Au NP deposition on each SiO_2 colloid. Initially, the fluid drop has a large equilibrium contact angle on each SiO_2 colloid due to poor wetting. A layer of air (vapor) exists beneath the chloroform and in the interstices of the SiO_2 monolayer (*i.e.*, air in the gaps). If a macroscopic drop spans many closely sized spheres, the top has to be flat since the mean curvature has to be the same everywhere and thus, the fluid-air interface must be almost flat as shown in the initial fluid shape Figure 7a. The changes of the contact line position at the drying front are indicated by arrows in Figure 7a–c. During drying, the contact line on a SiO_2 colloid tilts. Thus, any NPs bound to the sphere at the contact line would be left without solvent on each SiO_2 sphere resulting in ring formation by NP deposition (Figure 7d). Based on the motion of droplet shrinkage (Movie S1), when evaporation occurs, the contact line at the outer perimeter of the drop can no longer be horizontal (Figure 7b); the meniscus must curve inward. This inward curvature tends to displace the contact line inward until it is no longer stable. The unstable contact line then retracts inward to the neighboring spheres until it reaches a stable geometry, as shown in Figure 7c.[34] This retraction process continues until the entire macroscopic drop has fully retreated and evaporated leaving SiO_2 colloids decorated with Au NP rings (Figure 7d).

In the region where no evaporation occurs, we interpret ring formation at the contact line as follows. Due to the attractive

DOI: 10.1021/acsnano.6b04965
ACS Nano 2016, 10, 8947–8955

particle-interface interaction, the NPs absorb strongly to the liquid–air interface, forming a dense monolayer extending to the SiO_2 sphere (shown in Figure 7b,e).[35,36] The adsorbed layer decreases the air–solvent interfacial energy. Over time, the adsorption increases (Figure 7f), thus causing the contact line to rise on the spheres (indicated as black arrows in Figure 7c,g), and NPs at the contact line are pushed onto the sphere (Figure 7h). If the sphere is sufficiently hydrophilic, the particles may remain where they were deposited and if there are enough Au NPs the contact line will rise causing multiple concentric rings to form (Figures 4f and 7h). The differences seen with Au@DDT NPs result from the fact that these particles do not adsorb on the air–solvent interface and are not pushed to and pinned at the chloroform-SiO_2 contact line.

In addition, this model also suggests that the spheres that get dewetted early in the process should look different from those that get dewetted late due to the change of Au NP concentration. NP adsorption at the liquid–air interface is not only at the bottom but also on the top of the droplet.[35] As shown in Figure S4a, instead of ring formation, dense monolayers of NPs were observed in the center of the sample. SEM images taken from the inner region to the edge of the sample are shown in Figure S4. Figure S4e indicates the locations on the sample for the corresponding SEM images. These results also agree with our model. The innermost area (a in Figure S4e) should contain the highest density of Au NPs (Figure S4a). The outermost region (Figure S 4d) not only has the lowest density of Au NPs but also indicates the shrinkage direction of the droplet. As indicated in Figure S4d, spheres to the right side of the red curve have incomplete Au NP ring formation, while spheres to the left of the curve have complete ring formation, which indicates that the spheres on the right get dewetted earlier than spheres on the left side.

CONCLUSIONS

We presented a simple drop evaporation method to assemble chemically functionalized Au NPs into large arrays of ring structures on locally curved surfaces, in this case SiO_2 colloids. The large wettability change of chloroform is caused by both the temperature and relative humidity in the system. Controlled condensation of water on SiO_2 spheres is crucial for changing the contact angle of the hydrophobic chloroform solvent. The formation of Au NP ring structures on top of individual SiO_2 spheres is influenced by the distance between SiO_2 spheres and local heterogeneity in sphere size and ordering. The facile deposition of Au NP rings is a scale-free approach that can be utilized on monolayers of SiO_2 spheres with various diameters. Moreover, the ligands on these Au NPs determine whether one obtains the Au NP ring morphology or compact multiparticle mounds on the SiO_2 colloids. That the SiO_2 colloids are readily removed from the Si substrate, but the Au NP structures remain intact on each SiO_2 colloid, would facilitate experiments with Janus-like particles. This self-organization method is applicable to other NPs, *i.e.*, silver, CdSe NPs, *etc.* The large arrays of NP rings formed can be used in a variety of fields. We expect these ring structures to have interesting photonic properties that we will report elsewhere.

METHODS

Materials and Methods. The silica (SiO_2) spheres, citrate-stabilized gold NPs and methyl-PEG-thiol compounds were purchased from Fisher Scientific. Silicon wafers were obtained from Ted Pella, Inc. Nanopure water with a resistivity of 18 MΩ was used in all experiments. The preparation of methyl-PEG4-thiol-modified Au NPs, the characterization of the chemical modification of the Au NPs and the Langmuir–Blodgett self-assembly of colloidal SiO_2 monolayer films on Si substrates are described in detail in the Supporting Information (SI). The Scotch tape used to remove the monolayer of SiO_2 sphere is 3 M 600 transparent Scotch tape (model no. S-9782).

Preparation of Methyl-PEG4-Thiol-Modified Gold NPs (Au@MT(PEG)$_4$ NPs). The colloids used for these studies are methyl terminated $(PEG)_4$-thiol-modified 10 nm Au NPs (Au@MT$(PEG)_4$ NPs) dispersed in chloroform solvent. The purchased Au NPs were initially stabilized by citrate buffer. Surface modification of citrate coated Au NPs was conducted as follows. Approximately 10 mL Au@citrate solution (concentration 6.0×10^{12} particles/ml) and 10 mL of MT$(PEG)_4$ (w/v:1%) aqueous solution were added to a 20 mL vial. The solution was vigorously stirred for a minimum of 5 h, but typically overnight. The Au NPs were then collected *via* a high-speed centrifugation and redispersed in methanol and well suspended by mild sonication. The Au NPs were collected again *via* high-speed centrifugation and then well redispersed in chloroform solvent by mild sonication. Unlike citrate ligand, which undergoes dynamic exchange with free molecules in solution to stabilize Au NPs, methyl terminated $(PEG)_4$ thiol is covalently bonded to the surface of a Au NP and can stabilize Au NPs even when no free surfactant is present. The highest number density used in the experiment is 31.5×10^{13} particles/mL. The chloroform solution droplet is about 50 μL.

Experimental Set up and Procedure. The set up for fabricating Au NP coatings and rings on the SiO_2 spheres is illustrated schematically in Figure 1a. In the experiment, the SiO_2 monolayer fabricated on the Si substrate was placed in a Petri dish with its temperature (hence that of the substrate) controlled. A drop of Au NPs in chloroform solution was placed on the SiO_2 monolayer and allowed to evaporate under controlled conditions. Various Au NP films and ring structures remained after the solvent has completely evaporated and adhere to the SiO_2 colloidal particles (Figure 1b).

Characterization of Au NP Surface Modification. The ζ potential of the Au NPs was characterized using a Zeta analyzer (Malvern Instrument Ltd.). Changes in the ζ potential were taken as evidence for the modification of the Au NP surfaces. As shown in Table S1, Au@MT$(PEG)_4$ NPs exhibit a positive ζ potential (+43.6 mV) which is dramatically different from the pristine Au NPs that have a negative charge (−23.9 mV) due to the citrate coating. The change of ζ potential for Au NPs clearly reveals the replacement of MT$(PEG)_4$ ligands on the surface of Au NPs during the ligand exchange process. Au@MT$(PEG)_4$ NPs have an average diameter (±SD) of 17.0 ± 6.7 nm as determined by dynamic light scattering. This value is slightly smaller than that of the original NPs, which could be due to the large change of the dielectric constant of the solvents (from water (80.1) to chloroform (4.81) at 20 °C) and compression of the electrical double layer.[37]

Langmuir–Blodgett (LB) Assembled SiO_2 Sphere Monolayer. Silicon-wafer substrates, typical size of 10 × 10 mm, were first treated with piranha solution [3:1 (v/v) H_2SO_4/H_2O_2] for 30 min. Attention: Piranha solution is extremely dangerous and should be handled very carefully. After cleaning, the substrates were rinsed with Nanopure water at least three times and then stored in Nanopure water until use. The SiO_2 sphere monolayer films were prepared in a LB trough (Nima technologies).[38] First, 1 mL, 10 wt % SiO_2 solution was collected by centrifugation and well redispersed in methanol by sonication. This process was repeated two times, and finally the SiO_2 spheres were dispersed in 2 mL of methanol after few minutes of sonication. Then, 3 mL chloroform solvent was added to the SiO_2 sphere solution, and the final solution was sonicated and well mixed for 10 min. In order to prepare the SiO_2 sphere monolayer, a 1 mL $CHCl_3$/Methanol (v/v:3/2) solution of SiO_2 spheres was dropwise deposited on the water subphase surface of a LB trough and allowed to spread. The solvent was allowed to fully evaporate for 30 min. Then, the SiO_2 nano- to microparticles on the water–air interface were compressed by barriers until achieving a target pressure of about 12 mN/m. To fabricate the monolayer films of SiO_2 spheres on Si substrates, the Langmuir layer was transferred to the precleaned silicon

DOI: 10.1021/acsnano.6b04965
ACS Nano 2016, 10, 8947–8955

substrate while holding the surface pressure constant. We could continuously transfer the SiO_2 particle films onto at least 10 separate substrates from the LB trough in a single deposition operation.

ASSOCIATED CONTENT

Supporting Information

The Supporting Information is available free of charge on the ACS Publications website at DOI: 10.1021/acsnano.6b04965.

Experimental details and data (PDF)

Motion of a chloroform drop shape and volume during evaporation at 21 °C and ∼50% RH (AVI)

AUTHOR INFORMATION

Corresponding Author

*Email: nfschere@uchicago.edu.

Author Contributions

Y. B. and N.F.S. designed the research. Y.B. performed all the experiments. T.A.W. provides the geometrical theory. Y.B., T.A.W. and N.F.S. discussed results and wrote the manuscript.

Notes

The authors declare no competing financial interest.

ACKNOWLEDGMENTS

This work was supported by a grant from National Security Science and Engineering Faculty Fellowship (NSSEFF) from the U.S. Department of Defense. We thank the University of Chicago NSF-MRSEC (DMR-0820054) for central facilities support. We thank Di Liu for helpful discussions.

REFERENCES

(1) You, Y. Z.; Yu, Z. Q.; Cui, M. M.; Hong, C. Y. Preparation of Photoluminescent Nanorings with Controllable Bioreducibility and Stimuli-responsiveness. *Angew. Chem., Int. Ed.* **2010**, *49*, 1099−1102.

(2) Wang, L.; Lou, Z.; Wang, R.; Fei, T.; Zhang, T. Ring-like PdO-NiO with Lamellar Structure for Gas Sensor Application. *J. Mater. Chem.* **2012**, *22*, 12453−12456.

(3) Ragi, P. M.; Umadevi, K. S.; Nees, P.; Jose, J.; Keerthy, M. V.; Joseph, V. P. Flexible Split-Ring Resonator Metamaterial Structure at Microwave Frequencies. *Microw. Opt. Technol. Lett.* **2012**, *54*, 1415−1416.

(4) Liu, L.-N.; Duquesne, K.; Oesterhelt, F.; Sturgis, J. N.; Scheuring, S. Forces Guiding Assembly of Light-Harvesting Complex 2 in Native Membranes. *Proc. Natl. Acad. Sci. U. S. A.* **2011**, *108*, 9455−9459.

(5) Book, L. D.; Ostafin, A. E.; Ponomarenko, N.; Norris, J. R.; Scherer, N. F. Exciton Delocalization and Initial Dephasing Dynamics of Purple Bacterial LH2. *J. Phys. Chem. B* **2000**, *104*, 8295−8307.

(6) Wen, Z. C.; Wei, H. X.; Han, X. F. Patterned Nanoring Magnetic Tunnel Junctions. *Appl. Phys. Lett.* **2007**, *91*, 122511.

(7) Swanglap, P.; Slaughter, L. S.; Chang, W.-S.; Willingham, B.; Khanal, B. P.; Zubarev, E. R.; Link, S. Seeing Double: Coupling between Substrate Image Charges and Collective Plasmon Modes in Self-Assembled Nanoparticle Superstructures. *ACS Nano* **2011**, *5*, 4892−4901.

(8) Wen, F.; Ye, J.; Liu, N.; Van Dorpe, P.; Nordlander, P.; Halas, N. J. Plasmon Transmutation: Inducing New Modes in Nanoclusters by Adding Dielectric Nanoparticles. *Nano Lett.* **2012**, *12*, 5020−5026.

(9) Zhang, Q.; Wen, X.; Li, G.; Ruan, Q.; Wang, J.; Xiong, Q. Multiple Magnetic Mode-Based Fano Resonance in Split-Ring Resonator/Disk Nanocavities. *ACS Nano* **2013**, *7*, 11071−11078.

(10) Bozhevolnyi, S. I.; Volkov, V. S.; Devaux, E.; Laluet, J.-Y.; Ebbesen, T. W. Channel Plasmon Subwavelength Waveguide Components including Interferometers and Ring Resonators. *Nature* **2006**, *440*, 508−511.

(11) Li, S. P.; Peyrade, D.; Natali, M.; Lebib, A.; Chen, Y.; Ebels, U.; Buda, L. D.; Ounadjela, K. Flux Closure Structures in Cobalt Rings. *Phys. Rev. Lett.* **2001**, *86*, 1102−1105.

(12) Földi, P.; Kálmán, O.; Benedict, M. G.; Peeters, F. M. Networks of Quantum Nanorings: Programmable Spintronic Devices. *Nano Lett.* **2008**, *8*, 2556−2558.

(13) Wolf, O.; Campione, S.; Benz, A.; Ravikumar, A. P.; Liu, S.; Luk, T. S.; Kadlec, E. A.; Shaner, E. A.; Klem, J. F.; Sinclair, M. B.; Brener, I. Phased-Array Sources Based on Nonlinear Metamaterial Nanocavities. *Nat. Commun.* **2015**, *6*, 7667.

(14) Chen, J.; Liao, W.-S.; Chen, X.; Yang, T.; Wark, S. E.; Son, D. H.; Batteas, J. D.; Cremer, P. S. Evaporation-Induced Assembly of Quantum Dots into Nanorings. *ACS Nano* **2009**, *3*, 173−180.

(15) Liu, X.; Gozubenli, N.; Choi, B.; Jiang, P.; Meagher, T.; Jiang, B. Templated Fabrication of Periodic Arrays of Metallic and Silicon Nanorings with Complex Nanostructures. *Nanotechnology* **2015**, *26*, 055603.

(16) Deegan, R. D.; Bakajin, O.; Dupont, T. F.; Huber, G.; Nagel, S. R.; Witten, T. A. Capillary Flow as the Cause of Ring Stains from Dried Liquid Drops. *Nature* **1997**, *389*, 827−829.

(17) Khanal, B. P.; Zubarev, E. R. Rings of Nanorods. *Angew. Chem., Int. Ed.* **2007**, *46*, 2195−2198.

(18) Grzelczak, M.; Vermant, J.; Furst, E. M.; Liz-Marzán, L. M. Directed Self-Assembly of Nanoparticles. *ACS Nano* **2010**, *4*, 3591−3605.

(19) Egusa, S.; Redmond, P. L.; Scherer, N. F. Thermally-Driven Nanoparticle Array Growth from Atomic Au Precursor Solutions. *J. Phys. Chem. C* **2007**, *111*, 17993−17996.

(20) Jin, R.; Egusa, S.; Scherer, N. F. Thermally-Induced Formation of Atomic Au Clusters and Conversion into Nanocubes. *J. Am. Chem. Soc.* **2004**, *126*, 9900−9901.

(21) Hosoi, A. E.; Kogan, D.; Devereaux, C. E.; Bernoff, A. J.; Baker, S. M. Two-Dimensional Self-Assembly in Diblock Copolymers. *Phys. Rev. Lett.* **2005**, *95*, 037801.

(22) Whitesides, G. M.; Grzybowski, B. Self-Assembly at All Scales. *Science* **2002**, *295*, 2418−2421.

(23) Han, W.; Byun, M.; Li, B.; Pang, X.; Lin, Z. A Simple Route to Hierarchically Assembled Micelles and Inorganic Nanoparticles. *Angew. Chem., Int. Ed.* **2012**, *51*, 12588−12592.

(24) Byun, M.; Han, W.; Li, B.; Xin, X.; Lin, Z. An Unconventional Route to Hierarchically Ordered Block Copolymers on a Gradient Patterned Surface through Controlled Evaporative Self-Assembly. *Angew. Chem., Int. Ed.* **2013**, *52*, 1122−1127.

(25) Han, W.; Li, B.; Lin, Z. Drying-Mediated Assembly of Colloidal Nanoparticles into Large-Scale Microchannels. *ACS Nano* **2013**, *7*, 6079−6085.

(26) Li, B.; Han, W.; Jiang, B.; Lin, Z. Crafting Threads of Diblock Copolymer Micelles *via* Flow-Enabled Self-Assembly. *ACS Nano* **2014**, *8*, 2936−2942.

(27) Janssen, D.; De Palma, R.; Verlaak, S.; Heremans, P.; Dehaen, W. Static Solvent Contact Angle Measurements, Surface Free Energy and Wettability Determination of Various Self-Assembled Monolayers on Silicon Dioxide. *Thin Solid Films* **2006**, *515*, 1433−1438.

(28) Weitz, D. A.; Huang, J. S.; Lin, M. Y.; Sung, J. Limits of the Fractal Dimension for Irreversible Kinetic Aggregation of Gold Colloids. *Phys. Rev. Lett.* **1985**, *54*, 1416−1419.

(29) Elimelech, M.; Gregory, J.; Jia, X.; Williams, R. A. Application of Simulation Techniques to Colloidal Dispersion Systems. In *Particle Deposition & Aggregation*; Butterworth-Heinemann: Woburn, MA, 1995; pp 402−425.

(30) Kim, A. Y.; Hauch, K. D.; Berg, J. C.; Martin, J. E.; Anderson, R. A. Linear Chains and Chain-Like Fractals from Electrostatic Heteroaggregation. *J. Colloid Interface Sci.* **2003**, *260*, 149−159.

(31) Nosonovsky, M.; Bhushan, B. Phase Behavior of Capillary Bridges: Towards Nanoscale Water Phase Diagram. *Phys. Chem. Chem. Phys.* **2008**, *10*, 2137−2144.

(32) Cai, Y.; Zhang Newby, B.-m. Marangoni Flow-Induced Self-Assembly of Hexagonal and Stripelike Nanoparticle Patterns. *J. Am. Chem. Soc.* **2008**, *130*, 6076−6077.

DOI: 10.1021/acsnano.6b04965
ACS Nano 2016, 10, 8947−8955

(33) Saner, C. K.; Lusker, K. L.; LeJeune, Z. M.; Serem, W. K.; Garno, J. C. Self-Assembly of Octadecyltrichlorosilane: Surface Structures Formed Using Different Protocols of Particle Lithography. *Beilstein J. Nanotechnol.* **2012**, *3*, 114−122.
(34) Bodiguel, H.; Doumenc, F.; Guerrier, B. Stick−Slip Patterning at Low Capillary Numbers for an Evaporating Colloidal Suspension. *Langmuir* **2010**, *26*, 10758−10763.
(35) Bigioni, T. P.; Lin, X.-M.; Nguyen, T. T.; Corwin, E. I.; Witten, T. A.; Jaeger, H. M. Kinetically Driven Self Assembly of Highly Ordered Nanoparticle Monolayers. *Nat. Mater.* **2006**, *5*, 265−270.
(36) Jiang, Z.; Lin, X.-M.; Sprung, M.; Narayanan, S.; Wang, J. Capturing the Crystalline Phase of Two-Dimensional Nanocrystal Superlattices in Action. *Nano Lett.* **2010**, *10*, 799−803.
(37) Kaszuba, M.; Corbett, J.; Watson, F. M.; Jones, A. High-Concentration Zeta Potential Measurements Using Light-Scattering Techniques. *Philos. Trans. R. Soc., A* **2010**, *368*, 4439−4451.
(38) Bardosova, M.; Pemble, M. E.; Povey, I. M.; Tredgold, R. H. The Langmuir-Blodgett Approach to Making Colloidal Photonic Crystals from Silica Spheres. *Adv. Mater. (Weinheim, Ger.)* **2010**, *22*, 3104−3124.

DOI: 10.1021/acsnano.6b04965
ACS Nano 2016, 10, 8947−8955